Hydrodynamical interpretation of angular momentum and energy transfer in atomic processes

S. Y. Ovchinnikov,[1,2,3] J. H. Macek,[2] and D. R. Schultz[1]
[1]*Department of Physics, University of North Texas, Denton, Texas 76203, USA*
[2]*Department of Physics and Astronomy, University of Tennessee, Knoxville, Tennessee 37496, USA*
[3]*Ioffe Physical Technical Institute, St. Petersburg 194021, Russia*
(Received 4 September 2014; published 24 December 2014)

Through the description of several simple atomic-scale systems for illustration, the hydrodynamical interpretation of results of solving the time-dependent Schrödinger equation is used to elucidate the fundamental processes of angular momentum and energy transfer. Connections are made between the hydrodynamical interpretation and conventional views such as interference of superpositions of states. Along with previous theoretical and experimental demonstration of the existence of the hydrodynamical signatures born in atomic-scale interactions and remaining in the asymptotic observables, these illustrations show the complementarity of the hydrodynamical and conventional pictures as well as additional insight provided by the former.

DOI: 10.1103/PhysRevA.90.062713 PACS number(s): 34.50.Fa, 32.80.Fb

I. INTRODUCTION

The connection between hydrodynamics and the evolution of quantum mechanical entities was made very early on. In fact, Madelung [1] gave the first hydrodynamical interpretation of quantum mechanics less than a year after the appearance of Schrödinger's equation and just five years later Dirac [2] was the first to state the possibility of zeros occurring in the wave function associated with vortices. Then, in 1952, Takabayashi [3] showed that solutions of the time-dependent Schrödinger equation (TDSE) represent flows of compressible perfect fluids described by the Navier-Stokes equations. Much later, Bialynicki-Birula and collaborators showed that vortices are associated with singularities in the velocity field [4,5] and a theoretical prediction was made by the present authors of vortices that are created on the atomic scale and persist to asymptotic distances in ion-atom collisions [6], later confirmed by experiment [7], and in photon-atom interactions [8].

Furthermore, these recent results not only predicted the existence and detectability of hydrodynamical effects in atomic-scale interactions, but they began the elucidation of how the hydrodynamical interpretation could complement, and significantly add to, a more conventional interpretation of atomic-scale dynamics. Here we illustrate in more detail how hydrodynamics complements and extends interpretations based on interference of superpositions of states in atomic processes and provide a fuller understanding of angular momentum transfer in atomic collisions and energy transfer in photoionization.

II. ANGULAR MOMENTUM TRANSFER IN ION-ATOM COLLISIONS

The conventional view of how angular momentum is transferred from the external motion of the projectile to the target in ion-atom collisions involves the setting into rotation of the electronic probability density (in both bound and continuum states) and as the interference of the excited states populated in the collision (see Ref. [9] and a large portion of the literature interpreting alignment and orientation parameters in ion-atom collisions as coherent superpositions of states, e.g., Refs. [10–12]). To illustrate how the hydrodynamical interpretation adds to this picture, we consider a particularly simple system, the collision of an antiproton with atomic hydrogen. This system has no bound electronic states of the antiproton due to its charge sign. Therefore, it allows us to avoid complications of the interpretation involving the so-called two-center quasimolecular and continuum states in positive-ion impact and final states of the projectile (that is, the charge-transfer channel). In addition, there are no transitions on the incoming phase of the collision involving antiproton impact.

We accomplish this demonstration by solving the TDSE using lattice-based methods [13,14]. This approach provides a very accurate description, necessary to resolve clearly the zeros of the wave function associated with the formation and evolution of the vortices not as readily accomplished using other methods, for example, basis set expansion. Also, the lattice TDSE solutions are directly amenable to displaying the wave function as a function of time to allow elucidation of the origin and evolution of the hydrodynamical effects. In particular, we consider 5-keV antiproton impact of atomic hydrogen with an impact parameter $b = 1$ a.u. The resulting electronic probability density at several internuclear separations past the distance of closest approach ($R = 3$, 7.2, 33, and 167 a.u.) is shown in Fig. 1. This calculation is essentially a contemporary version of that which we carried out in 1996 to elucidate the mechanisms leading to the behavior of ionization of atoms by antiproton impact [15,16], for example, the dynamical exceeding of the Fermi-Teller limit at low energies, and which was confirmed by other authors (see, e.g., Ref. [17]).

Figure 1 shows the expected evolution of the wave function based on these previous works in which the antiproton excites the target electronic probability density, which expands in a roughly spherical distribution (as opposed to the shape formed by the two-center states, dominantly the σ-π distribution shown for positive-ion impact [18–22]), with a deep minimum surrounding the antiproton owing to the repulsion of the electronic probability density. We note that the dynamics displayed in Fig. 1 are quite similar over a relatively wide range of impact parameters, for example, $b = 0.4$–2 a.u. (as shown in previous work [16]).

To measure the angular momentum transfer in the collision, we compute the y projection of the expectation value of angular momentum $L_y = (\vec{r} \times \vec{p})_y = -i\hbar(\vec{r} \times \vec{\nabla})_y$ and display it in

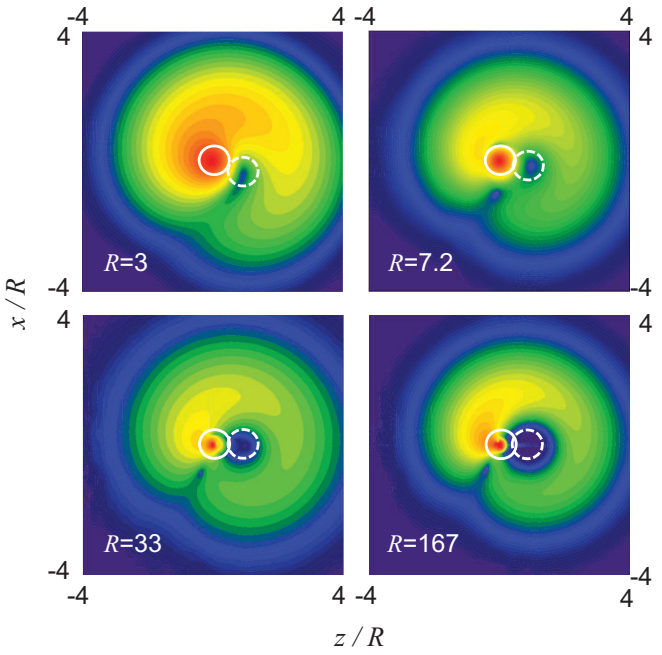

FIG. 1. (Color online) Two-dimensional slice of the electronic probability density for four internuclear distances (in a.u.) after the distance of closest approach in 5-keV antiproton impact of atomic hydrogen with $b = 1$ a.u. The impact parameter is in the $-x$ direction and the antiproton moves from $-z$ to $+z$ and is located at $(z,x) = (\sqrt{1-1/R^2}, -1/R)$, at the center of the white circle with a dashed line. The proton is located at $(z,x) = (0,0)$ at the center of the white circle with a solid line and the antiproton follows a trajectory in the scaled coordinates along a semicircle, centered at (0,0), with radius 1. The contours ranging from violet to red represent probability density from 10^{-4} to 10^{-1} for $R = 3$ a.u., $10^{-3.5}$ to $10^{0.5}$ for $R = 7.2$, 10^{-4} to 10^{1} for $R = 33$, and $10^{-3.5}$ to 1 for $R = 167$.

Fig. 2 as a function of distance along the antiproton trajectory (i.e., vt, where v is the antiproton velocity and t is time in a.u.). In addition, we decompose the curve into components owing to the angular momentum either about the origin of coordinates at the target nucleus or about the vortex centers. The former is accomplished by computing the center of mass of the electronic probability density and its angular velocity. Subtracting this rotation component from the total is the amount due to the vortices. As the figure illustrates, soon after the distance of closest approach, the dominant contribution comes from rotation of the electronic probability density; however, this overall rotation stops quickly and the subsequent increase in L_y comes from the vortices.

This can be seen by examination of the time evolution of not only the probability density but also the electronic probability current, as shown in Fig. 3. In particular, the panel showing these quantities at $R = 3$ a.u. shows that soon after the distance of closest approach there is a general expansion of the electronic probability density, owing to the reduced effective attraction of the electron by the target proton by the presence of the oppositely charged projectile, and a general rotation of the distribution set in motion by the repulsive push from the antiproton with a finite lever arm b. Then, as shown in the next panel, by $R = 7.2$ a.u., the general rotation has

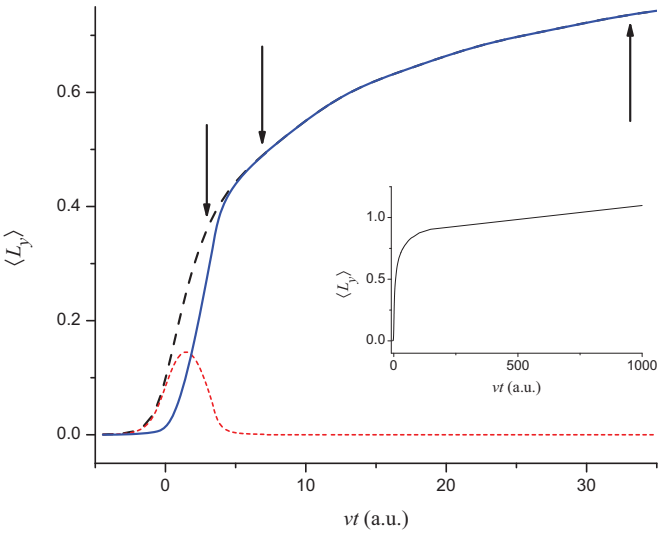

FIG. 2. (Color online) The y projection of angular momentum as a function of the distance vt along the antiproton trajectory in 5-keV antiproton impact of atomic hydrogen with $b = 1$ a.u. The red (short-dashed) curve is the portion of L_y due to rotation of the electronic probability density, the blue (solid) curve is that due to the rotation about the centers of vortices, and the black (dashed) curve is the total. The arrows indicate positions at which the electronic probability density and current are displayed in Fig. 3.

stopped and a ring vortex has formed. It occurs when there is a sufficient population of excited states built up (recall that we have noted that, unlike in positive-ion impact, there are no transitions on the incoming phase of the collision). This buildup results in an interference of the superposition of

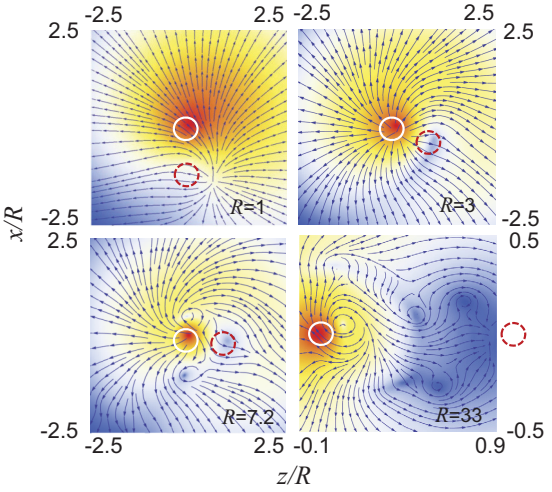

FIG. 3. (Color online) Electronic probability density (color contours) and probability current (arrows) for $R = 1$ a.u. and the three antiproton positions indicated in Fig. 2, showing the expansion with no vortices ($R = 1,3$ a.u.), rotation of the probability density as a whole and the presence of vortices ($R = 7.2$ a.u.), and the lack of rotation but continued creation and evolution of vortices ($R = 33$ a.u.). The position of the proton is at the center of the white circle and that of the antiproton is at the center of the red (dashed) circle. The contours represent the same levels as in Fig. 1.

the ground and excited states, corresponding as well to the region of low pressure. Specifically, the first vortex forms at $R \approx 4.5$ a.u., followed by another ring vortex at $R \approx 6.8$ a.u., with several more appearing at larger R. Again, we note that the dynamics of this system only weakly depend on impact parameter.

At $R \sim 7$ a.u. or more, the dominant contribution to the transfer of angular momentum for antiproton impact shifts from owing to rotation about the target nucleus to rotation about the vortex centers. The subsequent appearance of additional vortices, as shown for $R = 33$ a.u. in the figure, adds to the circulation of the electronic probability current about their centers. As time progresses, vortices interact, merging for example, and migrate to smaller radial distances from the target nucleus, leading to a further increase in angular momentum transfer until an asymptotic value is reached.

For positive-ion impact, we found [6] that on the outgoing phase of the collision formation of ring vortices corresponded to internuclear distances at which hidden crossings occurs. Hidden crossings are points in the complex plane of the adiabatic quasimolecular electronic potential energy surfaces corresponding to strong localized transitions (connections of one surface to another corresponding to different excited bound and continuum states). That is, we found a concurrence of the interference picture in which angular momentum transfer occurs when a sufficient population of excited states build up in order to interfere, corresponding to the hidden crossings distances, and the hydrodynamical picture in which the angular momentum transfer takes place when regions of low-pressure accrete vortices (at zeros of the wave function) with corresponding rotation of the electronic probability current around the vortex centers. For antiproton impact, there are no hidden crossings and the transitions are nonadiabatic.

III. MODEL SYSTEM FOR THE HYDRODYNAMICAL INTERPRETATION

The mechanism of angular momentum transfer through vortex creation and subsequent dynamical evolution, as well as the complementarity of the hydrodynamical interpretation and the picture involving interference of the superposition of states, can be further illustrated using a very simple model. Consider the time-dependent superposition of two atomic states H($1s_0$) and H($2p_+$), that is, $\psi(t) = A\varphi_{1s}e^{-iE_{1s}t} + B\varphi_{2p_+}e^{-iE_{2p_+}t}$, shown in Fig. 4 for four times $t = 0$, $\pi/2$, π, and $3\pi/2$, representing one cycle of the rotation of the deep minima about the nucleus seen in the figure. In terms of the interference picture, the superposition of the two states leads to the pattern of maxima and minima of the electronic probability density and the rotation of the distribution.

Next, consider the hydrodynamical interpretation in which the fluid is described by the TDSE as a limiting case of the Navier-Stokes equations. In particular, for an ideal, compressible fluid, if the viscosity vanishes and we assume that the equation of state (connecting the density $\rho = |\Psi|^2$ and the pressure p) for a compressible fluid is

$$\vec{\nabla} p = -\tfrac{1}{4}\rho\vec{\nabla}\left[(\nabla^2\rho)/\rho - \tfrac{1}{2}(\vec{\nabla}\rho)^2/\rho^2\right],$$

then the Navier-Stokes equations reduce to the TDSE. (While the pressure is, in general, a tensor, a more convenient measure for graphical display is the mean pressure [3] $\bar{p} = -\frac{\rho}{12}\nabla^2 \ln \rho$, which we utilize in the figures below.) The fluid flow equation (Euler's equation in this case) has vortex solutions when $\mathrm{Re}(\Psi) = 0 = \mathrm{Im}(\Psi)$, such that two nodal surfaces intersect along a curve and can result in zeros where the velocity field $\vec{v} = \mathrm{Im}\vec{\nabla}(\ln\Psi)$ diverges. Furthermore, the circulation is quantized, with $\oint \vec{v}\cdot d\vec{l} = 2\pi$. Important to note is the fact that for the wave function to vanish at a point as described here, it must carry some angular momentum, thus the intimate connection of the hydrodynamical interpretation and angular momentum transfer. Also important to note is the connection of the velocity field with the phase. In particular, the electronic probability current, which does not depend on the phase, related to the velocity by $\vec{j} = \rho\vec{v}$, does not diverge at the vortex centers since there the density goes to zero (i.e., at the vortex center $\rho \to 0$, $j \to 0$, $v \to \infty$).

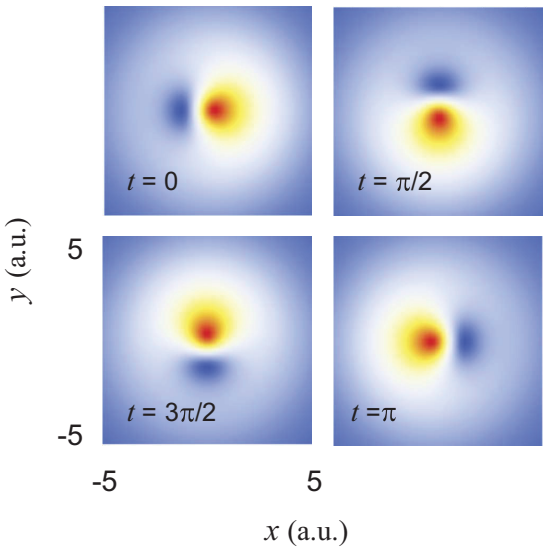

FIG. 4. (Color online) Model system displaying the presence of a vortex in the simple time-dependent superposition of two atomic states of hydrogen $A\varphi_{1s}e^{-iE_{1s}t} + B\varphi_{2p_+}e^{-iE_{2p_+}t}$, where $A = \sqrt{1-|B|^2} = 0.39$ and $B = 0.92$ with $z = 0$, $L_y = 0.84$, and $r_v = 1.58$ a.u., where r_v is the radial distance from the origin to the vortex. The contours ranging from blue to red represent probability density from 0 to 0.3.

As illustrated in Fig. 5 for the simple model, the deep minimum is formed at the resulting region of low pressure and moves to maintain its position in the low pressure. At the center of the minima is a zero of the wave function, with $\mathrm{Re}\psi = 0 = \mathrm{Im}\psi$, and the velocity field, illustrated in Fig. 5 by the electronic probability current, circulates about this point, constituting a vortex, and thus a rotation about a point away from the nucleus. That is, in contrast to the conventional picture in which the interference from the time-dependent superposition of the two states yields a rotation about the nucleus, the hydrodynamical interpretation shows that there is in addition a rotation about the vortex at the minima.

We can also relate the position of the vortex with the amount of angular momentum contributed by the rotation both about the vortex center and about the center of force. By varying the ratio A/B in the model wave function $\psi(t) =$

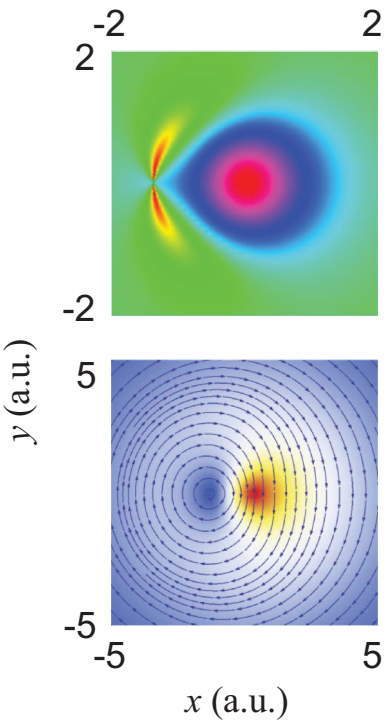

FIG. 5. (Color online) Pressure (top) and probability current (bottom) for the model system illustrating the location of the vortex at the minimum of pressure and the circulation about the center of the vortex. The color contours in the top panel represent levels from −0.03 to 0.7 from green to red and in the bottom panel from 0 to 0.3 for blue to red.

$A\varphi_{1s}e^{-iE_{1s}t} + B\varphi_{2p_+}e^{-iE_{2p_+}t}$, we can vary the radial distance from the nucleus of the vortex. In particular, normalization of the wave function requires that $|A| = \sqrt{1-|B|^2}$ and $\ell_z = \langle\psi|L_z|\psi\rangle = |B|^2$ (since $L_z\psi_{1s0} = 0$). Simple algebra then yields

$$\ell_z = \frac{1}{1+d_z}, \quad d_z = \frac{1}{64}\varrho^2 e^{r_v},$$

where r_v is the radial position of the vortex center, $\psi(r_v) = 0$, and $\varrho = \sqrt{x^2+y^2}$, so that when $z = 0$, $\varrho = r$. Figure 6 displays ℓ_z as a function of r_v, showing that the smaller the radial position of the vortex, the greater the angular momentum, being greatest when $A = 0$, $B = 1$, and thus $\psi = \varphi_{2p_+}$. Likewise, when r_v is large, the angular momentum is smallest, that is, when $A \to 1$ and $B \to 0$ corresponding to $\psi(t) = \varphi_{1s}$. The two components of ℓ_z, the rotation about the force center and the rotation about the vortex center, have opposite signs. As illustrated in the figure, the contribution from rotation about the force center, entering with a negative sign, is zero when r_v is zero, yielding $\ell_z = 1$ with the entire contribution from rotation about the vortex.

This simple model informs our interpretation of the richer dynamics present in the antiproton-hydrogen interaction. In particular, in that case, the initial state [H(1s)] has zero angular momentum, but gains some rotation as the repulsive interaction of the electronic cloud with the antiproton occurs as it approaches. However, the rotation stops once the antiproton has receded a short distance from the target and excitation

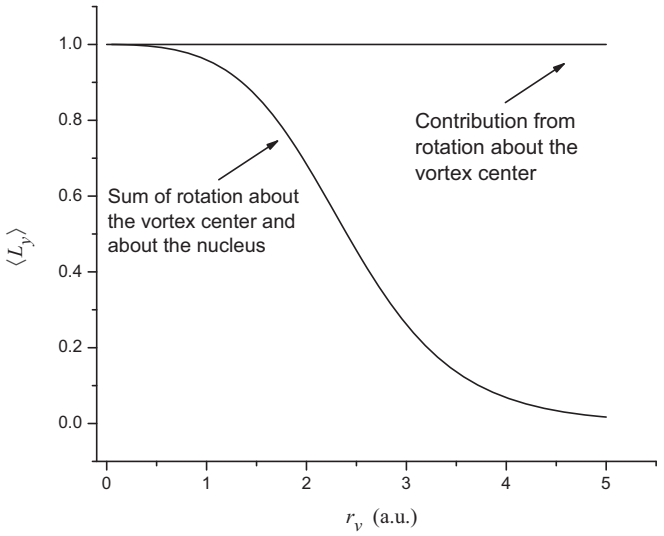

FIG. 6. Behavior of the y projection of angular momentum in the model system as a function of the distance from the nucleus to the center of the vortex r_v.

has built up sufficiently that a low-pressure region is created (corresponding to minima in the interference of the superposed states) so that a series of vortices form. Circulation about the vortices (as in the simple model) adds to the angular momentum, providing the dominant mechanism of angular momentum transfer from external motion of the antiproton relative to the target to internal electronic angular momentum. As the antiproton moves further away from the target as the ionized flux also moves away, the region of lower pressure becomes closer to the target center and the vortices migrate along with the motion of the low-pressure region closer to the target and (as in the simple model) the lower r_v drive the final increase of angular momentum asymptotically.

IV. HYDRODYNAMICAL INTERPRETATION OF ANGULAR MOMENTUM TRANSFER IN THE BORN APPROXIMATION

Another simple model that can be used to illustrate the formation of vortices in ion-atom collisions is the well-known Born approximation, specifically, the first-order Born approximation with incoming and outgoing plane waves. Valid at relatively high impact energies, the Born approximation has been a workhorse for computing excitation and ionization cross sections for many decades, yet, even when used to predict differential cross sections, for example, the ejected electron momentum distributions found using the reaction microscope [23,24] technique, typical Born approximation results do not display features readily attributable to vortex formation. One may therefore wonder if the hydrodynamical interpretation is not relevant for the high-energy collisions for which the Born approximation (or perturbation theory more generally) is presumably valid or if vortex formation is not as ubiquitous as we have suggested.

Remarkably, the Born approximation, found in standard textbooks (e.g., Refs. [25,26]), has no points at which the corresponding wave function vanishes, and thus can display

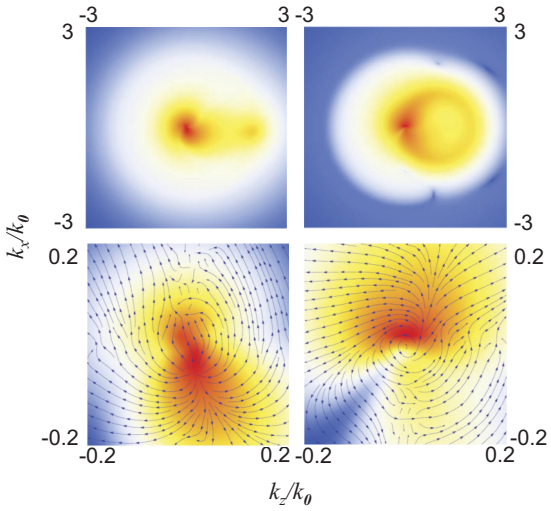

FIG. 7. (Color online) Two variants of the Born approximation for the ejected electron spectra in 400-keV proton impact of atomic hydrogen. The abscissa is the electron momentum in the z direction relative to $k_0 = m_e v$, where m_e is the electron mass and v is the projectile velocity, and the ordinate is the electron momentum in the x direction, similarly normalized by k_0. The left panels display the Born approximation for a proton scattering angle of 0.004°, with the top panel showing the electronic probability density and the bottom panel the pressure (color contours) and the probability current (arrows). The right panels display the impact-parameter-dependent Born approximation for $b = 1$ a.u., illustrating that this variant has sufficient detail to display the presence of vortex formation and evolution. The contours ranging from blue to red represent probability density from 10^{-5} to 10^{1} for the left-hand panels and from 10^{-6} to 10^{0} for the right-hand panels.

no vortices, and consequently there is no net transfer of angular momentum in this approximation. This is illustrated in the left-hand panels of Fig. 7, which display the electronic probability density in the top panel and the electronic probability current in the bottom panel for 400-keV proton impact of atomic hydrogen in the first-order plane-wave Born approximation.

Evidently, the Born approximation does not contain a rich enough description of the electronic dynamics to include these hydrodynamical features, which occurs since it does not correspond to a solution of the TDSE. To capture more of the dynamics that would be present in full solution of the TDSE, the Born approximation can be improved by including treatment of the impact parameter dependence of the ionization amplitude [27]. In particular, the well-known first-order Born $\mathcal{B}$ approximation of the ionization transition matrix element $T^{\mathcal{B}}(\vec{q})$ as a function of the momentum transfer $\vec{q}$, can be transformed to the impact-parameter-dependent transition amplitude by a two-dimensional Fourier transformation

$$a^{\mathcal{B}}(\vec{b},q_{\parallel}) = -i\,\frac{2\pi}{v}\int d^2\vec{q}_{\perp}e^{-i\vec{q}\cdot\vec{b}}T^{\mathcal{B}}(\vec{q}),$$

where v is the projectile velocity. The resulting ejected electron momentum distribution for this impact-parameter-dependent Born approximation, displayed for $b = 1$ a.u. in the right-hand panels of Fig. 7, shows the presence of vortices, indicated by the minimum of the electronic probability density seen there (which corresponds to a zero of the wave function) and the circulation about this point indicated by the electronic probability current. Thus, the sufficiently physically complete Born approximate does indeed manifest vortices that can persist to asymptotic distances and thus be potentially observable in experiments. Having predicted such surviving vortices for lower-energy ion-atom collisions [6] and extending the prediction for a more experimentally tractable, two-electron system $He^+ + He$ [28], we subsequently found that their position in the longitudinal ejected electron momentum distribution observable with finite scattering angle (and thus impact parameter) resolution can average out when summed over a range of impact parameters. Fortunately, we found that they are less sensitive to the sum over impact parameters in the transverse momentum distribution, enabling them to be found experimentally [7].

That is, when the vortex positions are reasonably insensitive to the range of impact parameters resolved, the reaction microscope technique is ideal for capturing images of the vortices that survive to asymptotic distances since they provide what amounts to an image of quasimolecular states formed in the ion-atom collision projected to asymptotic distances according to the imaging theorem. This theorem [27] states that when the wave function, initially localized in some region of space (i.e., after the accretion and near-collision evolution of the pressure and vortices), moves in the absence of forces, then it evolves linearly with time, implying that the probability density becomes proportional to the momentum distribution observed asymptotically.

Thus the reaction microscope technique images the σ-π distribution formed in one-electron (or effective one-electron) collisions in the top-of-barrier region [18–21] or the recently observed [7] σ-π-δ distribution when two-electron transitions are also important. We also point out, as has been previously noted [29], that vortex formation has been overlooked in electron-atom collisions as well, even when the corresponding deep minima in the angle and energy distribution of ejected electrons have been found experimentally [30] or theoretically [31–34]. In fact, it may be stated that the presence of vortices and the relevance of the hydrodynamical interpretation of atomic processes may have been noticed considerably earlier but that their presence has been obscured in previous methodology, for example, by insufficiently dynamically rich perturbation theory or in solution of the TDSE via basis set expansion with insufficiently high resolution of the deep minima. Vortices are thus likely ubiquitous in atomic processes but generally not recognized.

V. ENERGY TRANSFER IN PHOTOEXCITATION AND PHOTOIONIZATION OF ATOMS

The hydrodynamical interpretation of another important fundamental process, energy transfer, can be illustrated by considering the excitation and ionization of atoms by short laser pulses. In previous work [8], we considered a model system, a ~ 300 attosecond half-cycle electric-field pulse, and showed that its interaction with a target hydrogen atom displayed characteristics much like wind striking a building. That is, once the pulse had excited a significant population of $n = 2$ states, these interfered with the remaining ground-state

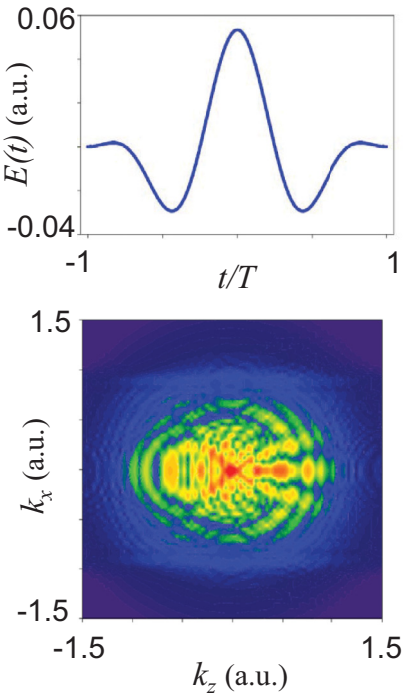

FIG. 8. (Color online) Ejected electron spectrum (bottom panel) resulting from photoionization of atomic hydrogen by the laser pulse illustrated in the top panel. The pulse has duration $T = 110.2$ a.u., an intensity of 10^{14} W/cm^2, and a laser wavelength of 800 nm. The contours in the bottom panel ranging from blue to red represent probability density from 10^{-2} to 5.

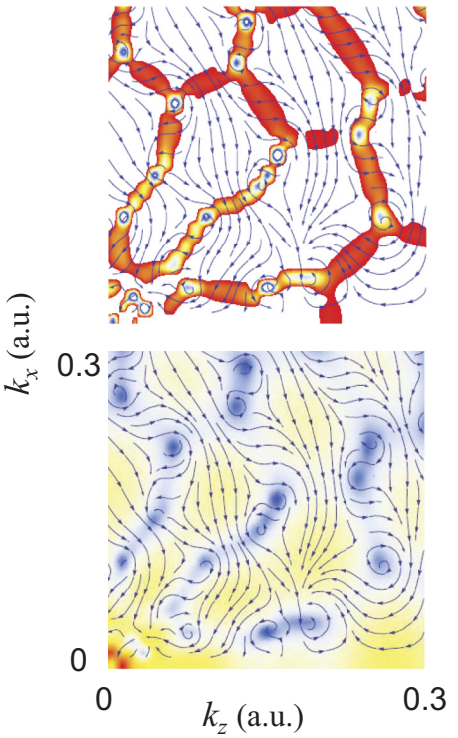

FIG. 9. (Color online) Illustration of the hydrodynamic character of the ejected electron spectrum in an enlarged area of that shown in Fig. 8. The bottom panel shows the electronic probability density, with minima (blue) at the positions of the vortex centers as demonstrated by the circulation of the probability current (arrows). The top panel further shows that the vortices are associated with low pressure (blue) and connected by filaments of tension (red). The contours ranging from blue to red represent probability density from 10^{-2} to 5 (bottom) and pressure from -0.3 to 0.15 (top).

population, accreting a ring vortex in the layer of low pressure created by the pulse on one side of the atom, which was then shed by the atom, moving off downstream much as a vortex created by the wind would be shed by a building or airfoil. Here we consider the extension of this to a full-cycle pulse, identical to that treated by other authors for comparison of the final results. Specifically, we have again used the regularized, scaled lattice TDSE method [14] to describe the time evolution of the wave function for a linearly polarized pulse of ~100-a.u. duration as depicted in the top panel of Fig. 8, which has also been considered by Chen *et al.* [35].

The resulting electronic momentum distribution for photoionization, as would be observed in a reaction microscope experiment, is shown in the bottom panel of Fig. 8 and is in accord with the results of Chen *et al.* What is seen is a complicated pattern of minima and maxima that are often interpreted as arising from interference of the states excited by the pulse. This is certainly true, but what we find by examining the time sequence of TDSE solutions is that just as in the case of the half-cycle pulse, they come about as a series of vortices accreted and driven by the pressure field. Specifically, the first rise of the field during the pulse begins to create an excited-state population that superposes with the ground state to accrete a series of ring vortices in the layer of low pressure that are successively shed from the atom and move downstream. As the field reverses sign during the continuation of the pulse, the vortices are driven back in the opposite direction simultaneous to the creation of another series of vortices on the opposite side of the atom that are shed in the new downstream direction. The number of vortices created on each rising or falling field segment of the pulse is proportional to the magnitude of the field in that segment, being proportional to the level of excitation produced.

To illustrate the complicated result of this process of vortex creation on either side of the atom and their subsequent evolution being driven in one direction and then the other, interacting with one another via mergers and annihilations, we display in Fig. 9 an enlarged portion of the final electronic momentum distribution. The bottom panel shows the electronic probability density as color contours, indicating the minima and maxima of density, along with the electronic current density, indicating the circulation about the zeros at the center of the minima. Thus, the minima in the full, complex ejected electron distribution not only are the resulting interference pattern of the excited states created by the pulse, but are vortices. It is important to note that sufficient accuracy of the numerical treatment is necessary to resolve the centers of the minima as being actual zeros to demonstrate that these are vortices.

The top panel of Fig. 9 displays the pressure field, with the colors indicating positive and negative values corresponding to pressure or tension. The minima of pressure correspond to the vortex positions, which are seen to be connected via a web of high and low pressure, the high-pressure regions corresponding to confluences of the electronic probability current.

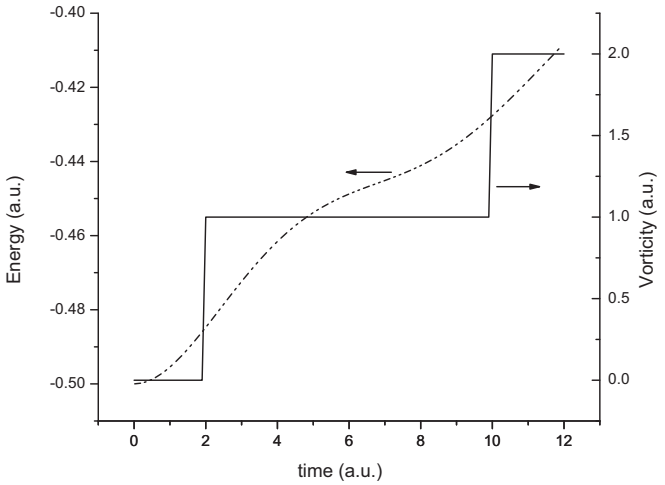

FIG. 10. Evolution of the electronic energy (dash–double-dotted curve, left scale) during the laser pulse and afterward to asymptotic time showing the mediation of the energy transfer from the pulse to the atom mediated by the creation and evolution of the vorticity (solid curve, right scale).

To illustrate the role vortex formation and evolution play in energy transfer, we have computed the energy (as given by the expectation of the electronic Hamiltonian $\langle\mathcal{H}\rangle$) and the vorticity [defined as $\vec{\omega} = \vec{\nabla} \times \vec{v}$, where $\vec{v} = \mathrm{Im}\vec{\nabla}(\ln\Psi)$ is again the velocity field] as a function of time. The result, shown in Fig. 10 for the early portion of the laser pulse, shows the correlation of the change in energy with the sequential appearance of vortices (i.e., quantized increases in the vorticity). Thus, quantification of the vorticity provides a measure of the energy transfer, hydrodynamics associated with vortices acting as a vehicle for transferring energy of the laser field to the electronic states.

It is again worth mentioning that by recognizing that the pattern of minima and maxima seen in typical ejected electron spectra produced by photoexcitation and photoionization results not only via interference of the excited states populated but in accordance with the hydrodynamical view of the interaction. This allows additional insight into the mechanism of energy transfer and shows that production and evolution of vortices is likely a ubiquitous feature of atomic-scale interactions.

VI. CONCLUSION

As we have noted, the foundation of the hydrodynamical interpretation of quantum mechanics has been laid out over many years through pioneering work from Madelung to Bialynicki-Birula *et al.* [1–5]. Then, more recently, we uncovered the presence of vortices, born at the atomic scale, for systems of both fundamental and practical interest [6,8], and found clues to the roles such hydrodynamical entities play. We have also shown that certain of the vortices can persist to asymptotic distances where they can be observed, providing confirmation of these findings [7]. Extending these works, the present study has begun elucidation at a more detailed level of fundamental processes present in atomic-scale dynamics such as ion- and photon-atom interactions.

In particular, several specific observations have been made linking the hydrodynamical and conventional views of processes such as angular momentum and energy transfer and showing how additional insight can be derived from the hydrodynamical interpretation. To begin with, we have shown that there is a direct connection of the buildup of excitation during the atomic-scale interaction (e.g., a collision or interaction with a laser pulse) with the appearance of vortices. This links the conventional view of the origin of the deep minima of observed ejected electron spectra as originating from interference of the superposition of ground and excited states with the hydrodynamical interpretation of the accretion of vortices at nodal surfaces created in regions of low pressure. The hydrodynamical view further indicates that at these points the complex wave function has a zero and consequently there must be a vortex at that point. This fundamental result shows that apart from the conventional view of angular momentum transfer occurring through rotation about the centers of force, significant angular momentum is transferred (and in some instances the dominant contribution) from rotation about the vortex centers.

We have also shown that the vortices created move, sometimes merging or annihilating, following paths along low pressure. The contribution of the rotation about the moving vortices to the total angular momentum is inversely proportional to their distances from the centers of force, the rotation about each vortex being quantized. As they move following the lows of pressure, they may migrate towards the centers of force, yielding greater angular momentum even after vortex formation is complete. We have also found that creation of vortices helps mediate energy transfer and that the vorticity as a function of time is a measure of the energy transfer.

The role of the pressure, not ordinarily considered in atomic-scale dynamics, is, perhaps surprisingly, seen to play a central role. That is, the quantity most conventionally displayed and discussed, the electronic probability density, say, a time slice from the solution of the TDSE, does not alone indicated the future evolution of the system. Instead, a slice in time of the pressure field indicates how the system will evolve in the near future, for example, with lines of low pressure conducting the vortices and regions of high pressure accreting greater probability density, somewhat in analogy to the use of pressure maps in the forecasting of weather.

It is also worth reiterating that the present and previous work indicate that vortex formation is likely ubiquitous in atomic-scale dynamics and yet has been largely overlooked. Taking note of this is important because it means that the opportunity to utilize the hydrodynamical interpretation of atomic-scale processes exists and can provide both complementary and additional insight, as we have begun to illustrate here. As we have shown, some vortices survive to asymptotic distances and are observable in measurements. In instances in which they are present they certainly contribute to the dynamics, for example, being vehicles for angular momentum and energy transfer. Greater understanding of these fundamental processes can be of practical importance as well as fundamental interest since they underlie the dynamics in larger-scale systems such as how photons interact with molecules and how electrons are transported in materials. Beyond the greater understanding that the hydrodynamical view gives, it may also afford opportunities for new types of manipulation or control of elementary or complex systems.

[1] E. Madelung, Z. Phys. **40**, 322 (1927).
[2] P. A. M. Dirac, Proc. R. Soc. London Ser. A **133**, 60 (1931).
[3] T. Takabayashi, Prog. Theor. Phys. **8**, 143 (1952).
[4] I. Bialynicki-Birula, M. Kalinski, and J. H. Eberly, Phys. Rev. Lett. **73**, 1777 (1994).
[5] I. Bialynicki-Birula, Z. Bialynicka-Birula, and C. Śliwa, Phys. Rev. A **61**, 032110 (2000).
[6] J. H. Macek, J. B. Sternberg, S. Y. Ovchinnikov, T.-G. Lee, and D. R. Schultz, Phys. Rev. Lett. **102**, 143201 (2009).
[7] L. Ph. H. Schmidt, C. Goihl, D. Metz, H. Schmidt-Böcking, R. Dörner, S. Yu. Ovchinnikov, J. H. Macek, and D. R. Schultz, Phys. Rev. Lett. **112**, 083201 (2014).
[8] S. Yu. Ovchinnikov, J. B. Sternberg, J. H. Macek, T.-G. Lee, and D. R. Schultz, Phys. Rev. Lett. **105**, 203005 (2010).
[9] U. Fano and J. H. Macek, Rev. Mod. Phys. **45**, 553 (1973).
[10] R. Hippler, W. Harbich, M. Faust, and H. O. Lutz, J. Phys. B **21**, 103 (1988).
[11] J. R. Ashburn, R. A. Cline, P. J. M. van der Burgt, W. B. Westerveld, and J. S. Risley, Phys. Rev. A **41**, 2407 (1990).
[12] N. Anderson and K. Bartschat, *Polarization, Alignment, and Orientation in Atomic Collisions* (Springer, Berlin, 2000).
[13] D. R. Schultz, M. R. Strayer, and J. C. Wells, Phys. Rev. Lett. **82**, 3976 (1999).
[14] T.-G. Lee, S. Yu. Ovchinnikov, J. B. Sternberg, V. Chupryna, D. R. Schultz, and J. H. Macek, Phys. Rev. A **76**, 050701 (2007).
[15] D. R. Schultz, P. S. Krstic, C. O. Reinhold, and J. C. Wells, Phys. Rev. Lett. **76**, 2882 (1996).
[16] J. C. Wells, D. R. Schultz, P. Gavras, and M. S. Pindzola, Phys. Rev. A **54**, 593 (1996).
[17] X.-M. Tong, T. Watanabe, D. Kato, and S. Ohtani, Phys. Rev. A **64**, 022711 (2001).
[18] R. Dörner, H. Kehmliche, M. H. Prior, C. L. Cocke, J. A. Gary, R. E. Olson, V. Mergel, J. Ullrich, and H. Schmidt-Böcking, Phys. Rev. Lett. **77**, 4520 (1996).
[19] M. A. Abdallah, C. L. Cocke, W. Wolff, H. Wolf, S. D. Kravis, M. Stöckli, and E. Kamber, Phys. Rev. Lett. **81**, 3627 (1998).
[20] J. H. Macek and S. Yu. Ovchinnikov, Phys. Rev. Lett. **80**, 2298 (1998).
[21] D. R. Schultz, C. O. Reinhold, P. S. Krstic, and M. R. Strayer, Phys. Rev. A **65**, 052722 (2002).
[22] E. Y. Sidky and C. D. Lin, J. Phys. B **31**, 2949 (1998).
[23] R. Dörner, V. Mergel, O. Jagutzki, L. Spielberger, J. Ullrich, R. Moshammer, and H. Schmidt-Böcking, Phys. Rep. **330**, 95 (2000).
[24] J. Ullrich, R. Moshammer, A. Dorn, R. Dörner, L. Ph. H. Schmidt, and H. Schmidt-Böcking, Rep. Prog. Phys. **66**, 1463 (2003).
[25] L. D. Landau and E. M. Lifshitz, *Quantum Mechanics: Non-relativistic Theory*, translated by J. B. Sykes and J. S. Bell (Pergamon, Oxford, 1965).
[26] M. R. C. McDowell and J. P. Coleman, *Introduction to the Theory of Ion-Atom Collisions* (North-Holland, Amsterdam, 1970).
[27] A derivation of the TDSE in a form accounting for an appropriate translation factor describing electronic motion in the full projectile-target potential to asymptotic times, as well as the corresponding first Born approximation amplitudes accounting for the impact parameter dependence and projectile-target interaction, is given by J. H. Macek, in *Dynamical Processes in Atomic and Molecular Physics*, edited by G. Ogurtsov and D. Dowek (Bentham Science, Oak Park, 2012).
[28] S. Y. Ovchinnikov, J. H. Macek. L. Ph. H. Schmidt, and D. R. Schultz, Phys. Rev. A **83**, 060701(R) (2011).
[29] J. H. Macek, J. B. Sternberg, S. Y. Ovchinnikov, and J. S. Briggs, Phys. Rev. Lett. **104**, 033201 (2010).
[30] A. J. Murray and F. H. Read, Phys. Rev. A **47**, 3724 (1993).
[31] J. Berakdar and J. S. Briggs, Phys. Rev. Lett. **72**, 3799 (1994).
[32] J. Berakdar and J. S. Briggs, J. Phys. B **27**, 4271 (1994).
[33] J. Botero and J. H. Macek, Phys. Rev. A **45**, 154 (1992).
[34] J. Colgan, O. Al-Hagan, D. H. Madison, A. J. Murray, and M. S. Pindzola, J. Phys. B **42**, 171001 (2009).
[35] Z. Chen, T. Morishita, A.-T. Le, M. Wickenhauser, X. M. Tong, and C. D. Lin, Phys. Rev. A **74**, 053405 (2006).